Limits on light-speed anisotropies from Compton scattering of high-energy electrons

J.-P. Bocquet,[1] D. Moricciani,[2] V. Bellini,[3] M. Beretta,[4] L. Casano,[2] A. D'Angelo,[5] R. Di Salvo,[2] A. Fantini,[5]

D. Franco,[5] G. Gervino,[6] F. Ghio,[7] G. Giardina,[8] B. Girolami,[7] A. Giusa,[3] V.G. Gurzadyan,[9,10] A. Kashin,[9]

S. Knyazyan,[9] A. Lapik,[11] R. Lehnert,[12,*] P. Levi Sandri,[4] A. Lleres,[1] F. Mammoliti,[3] G. Mandaglio,[8]

M. Manganaro,[8] A. Margarian,[9] S. Mehrabyan,[9] R. Messi,[5] V. Nedorezov,[11] C. Perrin,[1] C. Randieri,[3]

D. Rebreyend,[1,†] N. Rudnev,[11] G. Russo,[3] C. Schaerf,[5] M.L. Sperduto,[3] M.C. Sutera,[3] A. Turinge,[11] and V. Vegna[5]

[1]*LPSC, UJF Grenoble 1, CNRS/IN2P3, INPG, 53 avenue des Martyrs 38026 Grenoble, France*
[2]*INFN Sezione di Roma TV, 00133 Roma, Italy*
[3]*INFN Sezione di Catania and Università di Catania, 95100 Catania, Italy*
[4]*INFN Laboratori Nazionali di Frascati, 00044 Frascati, Italy*
[5]*INFN Sezione di Roma TV and Università di Roma "Tor Vergata," 00133 Roma, Italy*
[6]*INFN Sezione di Torino and Università di Torino, 10125 Torino, Italy*
[7]*INFN Sezione di Roma I and Istituto Superiore di Sanità, 00161 Roma, Italy*
[8]*INFN Sezione di Catania and Università di Messina, 98166 Messina, Italy*
[9]*Yerevan Physics Institute, 375036 Yerevan, Armenia*
[10]*Yerevan State University, 375025 Yerevan, Armenia*
[11]*Institute for Nuclear Research, 117312 Moscow, Russia*
[12]*ICN, Universidad Nacional Autónoma de México, A. Postal 70-543, 04510 México D.F., Mexico*
(Dated: October 25, 2018)

The possibility of anisotropies in the speed of light relative to the limiting speed of electrons is considered. The absence of sidereal variations in the energy of Compton-edge photons at the ESRF's GRAAL facility constrains such anisotropies representing the first non-threshold collision-kinematics study of Lorentz violation. When interpreted within the minimal Standard-Model Extension, this result yields the two-sided limit of 1.6×10^{-14} at 95% confidence level on a combination of the parity-violating photon and electron coefficients $(\tilde{\kappa}_{o+})^{YZ}$, $(\tilde{\kappa}_{o+})^{ZX}$, c_{TX}, and c_{TY}. This new constraint provides an improvement over previous bounds by one order of magnitude.

Properties of the speed of light c, such as isotropy and constancy irrespective of the motion of the source, play a key role in physics. For example, they are instrumental for both the conceptual foundations as well as the experimental verification of Special Relativity, and they currently provide the basis for the definition of length in the International System of Units. It follows that improved tests of, e.g., the isotropy of light propagation remain of fundamental importance in physics.

Experimental searches for anisotropies in c are further motivated by theoretical studies in the context of quantum gravity: it has recently been realized that a number of approaches to Planck-scale physics, such as strings, spacetime-foam models, non-commutative field theory, and varying scalars, can accommodate minuscule violations of Lorentz symmetry [1]. At presently attainable energies, such Lorentz-breaking effects can be described by the Standard-Model Extension (SME), an effective field theory that incorporates both the usual Standard Model and General Relativity as limiting cases [2]. To date, the minimal Standard-Model Extension (mSME), which contains only relevant and marginal operators, has provided the basis for numerous tests of Special Relativity in a wide variety of physical systems [3, 4].

In this work, we will study photons and electrons in an environment where gravity is negligible. Lorentz violation is then described by the single-flavor QED limit of the flat-spacetime mSME [2, 5]. This limit contains the real, spacetime-constant mSME coefficients $(k_F)^{\mu\nu\rho\lambda}$, $(k_{AF})^\mu$, b^μ, $c^{\mu\nu}$, $d^{\mu\nu}$, and $H^{\mu\nu}$, which control the extent of different types of Lorentz and CPT violation. Note, however, that $c^{\mu\nu}$ and $\tilde{k}^{\mu\nu} \equiv (k_F)_\alpha{}^{\mu\alpha\nu}$ are observationally indistinguishable in a photon–electron system: suitable coordinate rescalings freely transform the $\tilde{k}^{\mu\nu}$ and $c^{\mu\nu}$ parameters into one another [5, 6]. Physically, this represents the fact that the speed of light is measured *relative* to the speed of electrons. We exploit this freedom by selecting the specific scaling $c^{\mu\nu} = 0$ in intermediate calculations. However, we reinstate this coefficient in the final result for generality.

From a phenomenological perspective, the dominant mSME coefficient is k_F, which causes a direction- and polarization-dependent speed of light [6]. Various of its components have been tightly bounded with astrophysical observations [7], Michelson–Morley tests [4, 8], and collider physics [5]. We will bound the $\tilde{\kappa}_{o+}$ piece of $\tilde{k}^{\mu\nu}$, which is an antisymmetric 3×3 matrix; it currently obeys the weakest limits, so all other mSME coefficients can be set to zero in what follows. An mSME analysis then reveals that the photon's dispersion relation is modified:

$$\omega = (1 - \vec{\kappa} \cdot \hat{\lambda})\lambda + \mathcal{O}(\kappa^2). \tag{1}$$

Here, $\lambda^\mu = (\omega, \lambda\hat{\lambda})$ denotes the photon 4-momentum and $\hat{\lambda}$ is a unit 3-vector. The three components of $\tilde{\kappa}_{o+}$

have been assembled into the form of a 3-vector: $\vec{\kappa} \equiv ((\tilde{\kappa}_{o+})^{23}, (\tilde{\kappa}_{o+})^{31}, (\tilde{\kappa}_{o+})^{12}) \equiv (\kappa_X, \kappa_Y, \kappa_Z)$. This vector specifies a preferred direction, which violates Lorentz symmetry; it can be interpreted as generating a direction-dependent refractive index of the vacuum $n(\hat{\lambda}) \simeq 1 + \vec{\kappa} \cdot \hat{\lambda}$. The electron's dispersion relation $E(p) = \sqrt{m^2 + p^2}$ remains unaltered with our choice of coordinate scaling.

The dispersion relation (1) shows that for a given λ, the photon energy ω depends on the direction $\hat{\lambda}$ of the photon's 3-momentum, which exposes the $\tilde{\kappa}_{o+}$ anisotropies. Reversing the direction of $\hat{\lambda}$ establishes parity violation in these anisotropies. The basic experimental idea is that in a terrestrial laboratory the photon 3-momentum in a Compton-scattering process changes direction due to the Earth's rotation. The photons are thus affected by the anisotropies in Eq. (1) leading to sidereal effects in the kinematics of the process. Precision measurements of Compton scattering of ultrarelativistic electrons circulating in a high-energy accelerator could help reveal such effects. In a previous paper [9], we have established the high sensitivity of a method based on the analysis of the Compton-edge (CE) energy (i.e., the minimal energy) of the scattered electrons using the GRAAL beamline [10] at the European Synchrotron Radiation Facility (ESRF, Grenoble, France). The present work utilizes dedicated GRAAL data and an improved set-up to extract a competitive bound on $\tilde{\kappa}_{o+}$ at the 10^{-14} level. Note that for the first time, kinematical non-threshold physics in a particle collision is exploited to test Lorentz symmetry: previous studies have employed predictions involving thresholds, such as shifts in thresholds (e.g., $\gamma\gamma \rightarrow e^+ e^-$), the presence of novel processes above certain thresholds (e.g., photon decay), or the absence of conventional collisions above certain thresholds (e.g., neutron stability) [11].

The experimental set-up at GRAAL involves counter-propagating incoming electrons and photons with 3-momenta $\vec{p} = p\,\hat{p}$ and $\vec{\lambda} = -\lambda\,\hat{p}$, respectively. The conventional CE then occurs for outgoing photons that are backscattered at $180°$, so that the kinematics is essentially one dimensional along the beam direction $\hat{p}$. Energy conservation for this process reads

$$E(p) + (1 + \vec{\kappa} \cdot \hat{p})\,\lambda = E(p - \lambda - \lambda') + (1 - \vec{\kappa} \cdot \hat{p})\,\lambda' \,, \quad (2)$$

where $\vec{\lambda}' = \lambda'\,\hat{p}$ is the 3-momentum of the CE photon, and 3-momentum conservation has been implemented. At leading order, the physical solution of Eq. (2) is

$$\lambda' \simeq \lambda_{CE}\left[1 + \frac{2\gamma^2}{(1 + 4\gamma\lambda/m)^2}\,\vec{\kappa} \cdot \hat{p} \right]. \quad (3)$$

Here, $\lambda_{CE} = \frac{4\gamma^2 \lambda}{1 + 4\gamma\lambda/m}$ denotes the conventional value of the CE energy. Given the actual experimental data of $m = 511\,\text{keV}$, $p = 6030\,\text{MeV}$, and $\lambda = 3.5\,\text{eV}$, yields $\gamma \simeq p/m = 11800$ and $\lambda_{CE} = 1473\,\text{MeV}$. The numerical value of the factor in front of $\vec{\kappa} \cdot \hat{p}$ is about 1.6×10^8. It
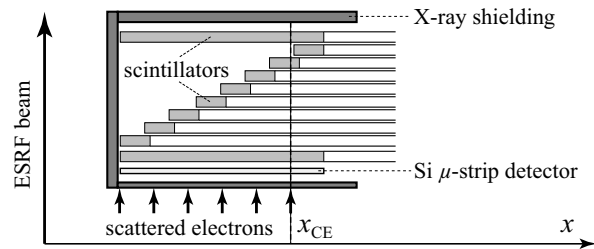

FIG. 1: Schematic drawing of the tagging system.

is this large amplification factor (essentially given by γ^2) that yields the exceptional sensitivity of the CE to $\tilde{\kappa}_{o+}$.

For comparisons between tests, mSME coefficients are conventionally specified in the Sun-centered inertial frame (X, Y, Z) [4], in which $\vec{\kappa}$ is constant, $\hat{Z}$ parallel to the Earth's rotation axis, and terrestrial laboratories rotate with a frequency $\Omega \simeq 2\pi/(23\,\text{h}\,56\,\text{min})$ about $\hat{Z}$. Hence, $\hat{p}(t) \simeq (0.9\cos\Omega t, 0.9\sin\Omega t, 0.4)$, where the beam direction of GRAAL has been used, and the time $t = 0$ has been chosen appropriately. Then, Eq. (3) becomes

$$\lambda' \simeq \tilde{\lambda}_{CE} + 0.91\,\frac{2\gamma^2\lambda_{CE}}{(1 + 4\gamma\lambda/m)^2}\sqrt{\kappa_X^2 + \kappa_Y^2}\,\sin\Omega t. \quad (4)$$

Here, we have absorbed the time-independent κ_Z piece into $\tilde{\lambda}_{CE}$ and dropped an irrelevant phase. Equation (4) clearly exposes the possibility of sidereal variations in the CE and represents our main theoretical result.

Small deviations $\delta\varphi$ from exactly counter-propagating incoming photons and electrons as well as the Lorentz-violating dispersion relation (1) itself can place the CE direction slightly off-axis. Moreover, Lorentz violation can affect laser lines as well as the spectrometer's B field. These effects have been carefully studied and shown to be negligible, so the primary Lorentz-violating effect in the present context is given by Eq. (4).

Incoming photons are generated by a high-power Ar laser located about $40\,\text{m}$ from the intersection region. The laser beam enters the vacuum via a MgF window and is then reflected by an Al-coated Be mirror towards the $6.03\,\text{GeV}$ electron beam. The laser and electron beams overlap over a $6.5\,\text{m}$ long straight section. Photons are finally absorbed in a four-quadrant calorimeter, which allows the stabilization of the laser-beam barycenter to $0.1\,\text{mm}$. This level of stability is necessary and corresponds to a major improvement of the set-up relative to our previous result. Due to their energy loss, scattered electrons are extracted from the main beam in the magnetic dipole following the straight section. Their position can then be accurately measured in the so-called tagging system (Fig. 1) located $50\,\text{cm}$ after the exit of the dipole. This system plays the role of a magnetic spectrometer from which we can infer the electron momentum. The tagging system is composed of a position-sensitive Si μ-strip detector (128 strips of $300\,\mu\text{m}$ pitch, $500\,\mu\text{m}$ thick) associated to a set of fast plastic scintillators for timing
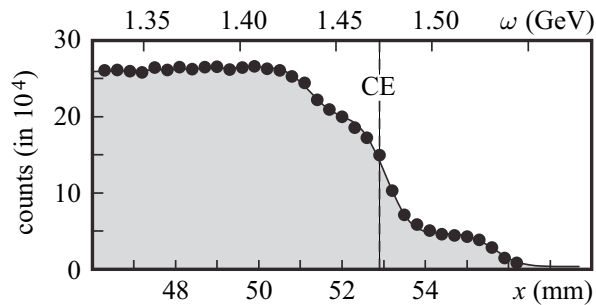
FIG. 2: Si μ-strip count spectrum near the CE and the fitting function (see text) vs. position x and photon energy ω. The three edges corresponding to the lines 364, 351, and 333 nm are clearly visible. The CE position x_{CE} is the location of the central line and is measured with a typical accuracy of $3\,\mu$m.

information and triggering of the DAQ. These detectors are placed inside a movable box shielded against the huge X-ray background generated in the dipole. A spring system ensures that the position-sensitive Si detector always touches the box end. As will be discussed later, the X-ray induced heat load is the origin of sizable variations in the box temperature, correlated with the ESRF beam intensity. This produces a continuous drift of the detector due to the dilation of the box.

A typical Si μ-strip count spectrum near the CE is shown in Fig. 2 for the multiline UV mode of the laser used in this measurement. This setting corresponds to 3 groups of lines centered around 364, 351, 333 nm, which are clearly resolved. The fitting function, also plotted, is based on the sum of 3 error functions plus background and includes 6 free parameters. The CE position, x_{CE}, is taken as the location of the central line. The steep slope of the CE permits an excellent measurement of x_{CE} with a resolution of $\sim 3\,\mu$m for a statistics of about 10^6 counts. The specially designed VIRTEX-II electronics [12] allowed us to collect such a statistics every 30 s, as compared to a few hours in our previous measurement.

During a week of data taking in July 2008, a total of 14765 CE spectra have been recorded. A sample of the time series of the CE positions relative to the ESRF beam covering 24 h is displayed in Fig. 3c, along with the tagging-box temperature (Fig. 3b) and the ESRF beam intensity (Fig. 3a). The sharp steps present in Fig. 3a correspond to the twice-a-day refills of the ESRF ring. The similarity of the temperature and CE spectra combined with their correlation with the ESRF beam intensity led us to interpret the continuous and slow drift of the CE positions as a result of the tagging-box dilation. To remove this trivial time dependence, we have fitted our raw data with the function

$$x_{fit}(t) = x_0 + a\left[1 - \exp(-t/\tau_1)\right]\exp(-t/\tau_2)\,,\quad (5)$$

where $t = 0$ is chosen appropriately, and τ_1, τ_2 are time constants describing heat diffusion and ESRF
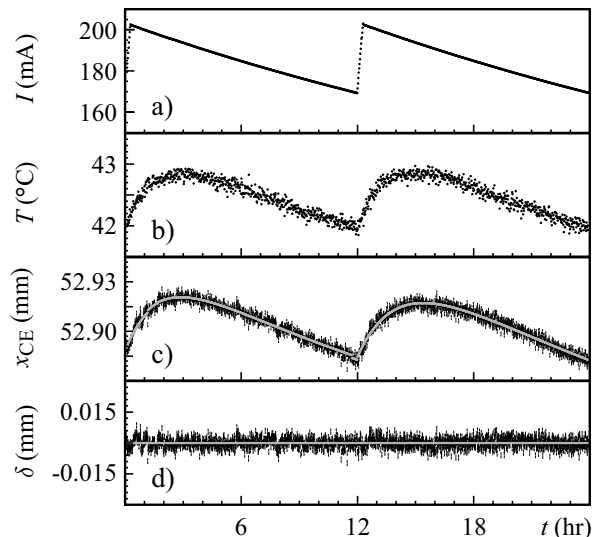

FIG. 3: Time evolution over a day of a) ESRF beam intensity; b) tagging-box temperature; c) CE position and fitted curve (Eq. 5); d) $\delta = x_{CE} - x_{fit}$. The error bars on position measurements are directly given by the CE fit.

beam-intensity decay, respectively. These two constants could be extracted directly from the temperature data (Fig. 3b). Consequently, each time series between two refills (12 h) has been fitted with only two free parameters: the position offset x_0 and the amplitude a. The corrected and final spectrum, obtained by subtraction of the fitted function from the raw data, is plotted in Fig. 3d.

This correction procedure is critical since its amplitude is 3 orders of magnitude larger than the extracted limit. To test its validity, the same analysis has been applied to simulated data obtained by adding a known harmonic oscillation to the experimental data. This study has shown that the signal amplitude would indeed be attenuated by a factor ranging from 1.3 to 2.3 depending on the phase.

The usual equation for the deflection of charges in a magnetic field together with momentum conservation in Compton scattering determines the relation between the CE position x_{CE} and the photon 3-momentum λ':

$$x_{CE} = \frac{\lambda'}{p - \lambda'}\,C\,,\quad (6)$$

where p is again the momentum of the ESRF beam. The constant C is determined by the trajectory of the electron; it therefore depends on the B-field magnitude and geometrical factors. Equation (6) can be used to derive the CE displacement resulting from a change in λ':

$$\frac{\Delta x_{CE}}{x_{CE}} = \frac{p}{p - \lambda_{CE}}\frac{\Delta\lambda'}{\lambda'}\,.\quad (7)$$

To search for a modulation, the 14765 data points have been folded modulo a sidereal day and divided in 24 bins (Fig. 4). The error bars are purely statistical and in agreement with a null signal ($\chi^2 = 1.04$ for the unbinned
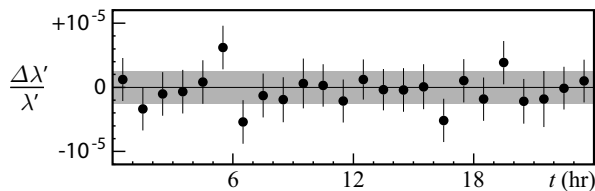
FIG. 4: Full set of data folded modulo a sidereal day (24 bins). The error bars are purely statistical and agree with the dispersion of the data points ($\chi^2 = 1.04$ for the unbinned histogram). The shaded area corresponds to the region of non-excluded signal amplitudes.

histogram). Moreover, the histogram has been Fourier analyzed and provides no evidence for a harmonic oscillation at the sidereal frequency. Hence, an upper bound on a hypothetical oscillation can be extracted. To exclude the signal hypothesis $A\sin(\Omega t + \phi)$ at a given confidence level (CL), a statistical analysis has been developed. In particular, we have chosen the Bayesian approach [13], which allows us to take into account the ϕ-dependent attenuation factor due to our correction procedure in a natural way. The p.d.f. for the amplitude of the signal is generated by incorporating directly the attenuation factor in the likelihood function before integration over ϕ. The resulting upper bound is $A < 2.5 \times 10^{-6}$ at 95% CL.

We next consider effects that could conceal an actual sidereal signal. Besides a direct oscillation of the orbit, the two quantities that may affect the result appear in Eq. (6): the dipole magnetic field via C, and the momentum of the ESRF beam p. All these parameters are linked to the machine operation, and their stability follows directly from the accelerator performance. At the ESRF, the electron orbit is precisely monitored to better than a μm, and the beam is maintained on its so-called golden orbit by adjustment of the RF-generator frequency. Access to the accelerator database has allowed us to analyze the time series of both the dipole magnetic field and the orbit position close to our tagging system. We have verified that the fluctuations of either parameter do not exceed 10^{-6}. The momentum stability of the ESRF beam, given by $\int B\,dl$, is then ensured to be better than 10^{-6}. We therefore estimate that a sidereal oscillation related to one of the machine parameters cannot exceed a few parts in 10^7 and is negligible.

We can now conclude that our upper bound on a hypothetical sidereal oscillation of the CE energy is:

$$\Delta\lambda'/\lambda' < 2.5 \times 10^{-6} \quad (95\,\%\,\text{CL})\,, \tag{8}$$

yielding the competitive limit $\sqrt{\kappa_X^2 + \kappa_Y^2} < 1.6 \times 10^{-14}$ (95 % CL) with Eq. (4). Reinstating mSME notation and the electron coefficients for generality gives at 95 % CL

$$\sqrt{[2c_{TX} - (\tilde{\kappa}_{o+})^{YZ}]^2 + [2c_{TY} - (\tilde{\kappa}_{o+})^{ZX}]^2} < 1.6 \times 10^{-14} \tag{9}$$

improving previous bounds by a factor of ten. The other, omitted mSME coefficients leave this limit unaffected.

In summary, we have made use of the GRAAL γ-ray beam produced by inverse Compton scattering off the high-energy electrons circulating in the ESRF ring to test the isotropy of light propagation. This represents the first test of Special Relativity via a non-threshold kinematics effect in a particle collision. Our measurement, based on the search for sidereal modulations in the CE of the scattered electrons, shows no evidence for a signal. Interpreting our result within the mSME, we have obtained a competitive upper bound on a combination of coefficients of the mSME's QED sector at the 10^{-14} level.

[*] ralf.lehnert@nucleares.unam.mx
[†] rebreyend@lpsc.in2p3.fr
[1] See, e.g., V.A. Kostelecký and S. Samuel, Phys. Rev. D 39, 683 (1989); J. Alfaro, H.A. Morales-Técotl, and L.F. Urrutia, Phys. Rev. Lett. 84, 2318 (2000); S.M. Carroll et al., Phys. Rev. Lett. 87, 141601 (2001); J.D. Bjorken, Phys. Rev. D 67, 043508 (2003); V.A. Kostelecký et al., Phys. Rev. D 68, 123511 (2003); F.R. Klinkhamer and C. Rupp, Phys. Rev. D 70, 045020 (2004); N. Arkani-Hamed et al., JHEP 0507, 029 (2005).
[2] D. Colladay and V.A. Kostelecký, Phys. Rev. D 55, 6760 (1997); Phys. Rev. D 58, 116002 (1998); V.A. Kostelecký and R. Lehnert, Phys. Rev. D 63, 065008 (2001); V.A. Kostelecký, Phys. Rev. D 69, 105009 (2004).
[3] For recent reviews see, e.g., V.A. Kostelecký, ed., CPT and Lorentz Symmetry I-IV, World Scientific, Singapore, 1999-2008; R. Bluhm, Lect. Notes Phys. 702, 191 (2006); D.M. Mattingly, Living Rev. Rel. 8, 5 (2005).
[4] V.A. Kostelecký and N. Russell, arXiv:0801.0287.
[5] M.A. Hohensee et al., Phys. Rev. Lett. 102, 170402 (2009); Phys. Rev. D 80, 036010 (2009); B.D. Altschul, Phys. Rev. D 80, 091901 (2009).
[6] V.A. Kostelecký and M. Mewes, Phys. Rev. Lett. 87, 251304 (2001); Phys. Rev. D 66, 056005 (2002).
[7] V.A. Kostelecký and M. Mewes, Phys. Rev. Lett. 97, 140401 (2006).
[8] S. Herrmann et al., in Ref. [3], Vol. IV; Ch. Eisele et al., Phys. Rev. Lett. 103, 090401 (2009); M.E. Tobar et al., Phys. Rev. D 80, 125024 (2009).
[9] V.G. Gurzadyan et al., Mod. Phys. Lett. A 20, 19 (2005).
[10] A description of the GRAAL facility can be found in O. Bartalini et al. [GRAAL Collaboration], Eur. Phys. J. A 26, 399 (2005) and references therein.
[11] R. Lehnert, Phys. Rev. D 68, 085003 (2003).
[12] G. Angeloni, Università di Roma "Tor Vergata" int. rep.
[13] C. Amsler et al. [Particle Data Group], Phys. Lett. B 667, 1 (2008).